

**Deterministic preparation of supersinglets with collective spin projections**Ebubechukwu O. Ilo-Okeke <sup>1,2</sup> Yangxu Ji,<sup>3,1</sup> Ping Chen,<sup>3,1</sup> Yuping Mao,<sup>3,1</sup> Manikandan Kondappan,<sup>3,1</sup> Valentin Ivannikov <sup>1,4</sup> Yanhong Xiao,<sup>5,6,7</sup> and Tim Byrnes<sup>1,3,4,8,9,10,\*</sup><sup>1</sup>*New York University Shanghai, 1555 Century Avenue, Pudong, Shanghai 200122, China*<sup>2</sup>*Department of Physics, School of Physical Sciences, Federal University of Technology, P. M. B. 1526, Owerri 460001, Nigeria*<sup>3</sup>*State Key Laboratory of Precision Spectroscopy, School of Physical and Material Sciences, East China Normal University, Shanghai 200062, China*<sup>4</sup>*NYU-ECNU Institute of Physics at NYU Shanghai, 3663 Zhongshan Road North, Shanghai 200062, China*<sup>5</sup>*State Key Laboratory of Quantum Optics and Quantum Optics Devices, Institute of Laser Spectroscopy, Shanxi University, Taiyuan, Shanxi 030006, China*<sup>6</sup>*Collaborative Research Center on Quantum Optics and Extreme Optics, Shanxi University, Taiyuan, Shanxi 030006, China*<sup>7</sup>*Department of Physics, State Key Laboratory of Surface Physics and Key Laboratory of Micro and Nano Photonic Structures (Ministry of Education), Fudan University, Shanghai 200433, China*<sup>8</sup>*National Institute of Informatics, 2-1-2 Hitotsubashi, Chiyoda-ku, Tokyo 101-8430, Japan*<sup>9</sup>*Center for Quantum and Topological Systems (CQTS), NYUAD Research Institute, The NYU Abu Dhabi (NYUAD), UAE*<sup>10</sup>*Department of Physics, New York University, New York, New York 10003, USA*

(Received 26 March 2022; accepted 31 August 2022; published 16 September 2022)

We introduce a procedure to generate supersinglets, the multipartite generalization of angular momentum singlet states. A supersinglet is defined as a total spin zero state consisting of  $N$  spin- $j$  particles. They are highly entangled and have zero spin variance in any direction, and as such are potentially useful for quantum metrology. Our scheme is based on projective measurements that measure the collective spin of the whole spin ensemble. A local unitary rotation is applied conditionally on the measurement outcome, such as to maximize the probability of obtaining spin zero on the subsequent measurement. The sequence is repeated in the  $z$  and  $x$  basis until convergence is obtained towards the supersinglet state. Our sequence works regardless of the initial state, and no postselection is required. Due to the use of strong projective measurements, very fast convergence towards zero spin variance is obtained. We discuss an example implementation using quantum nondemolition measurements in atomic ensembles, and perform numerical simulations to demonstrate the procedure.

DOI: [10.1103/PhysRevA.106.033314](https://doi.org/10.1103/PhysRevA.106.033314)**I. INTRODUCTION**

Entangled states in many-body systems have been of interest in several areas of modern physics, both from a scientific and application point of view. In condensed-matter physics and high-energy physics often one is interested in the low-energy states of a many-body Hamiltonian, which is often a highly entangled state [1–4]. In quantum information [5], they are the basis for numerous applications, such as quantum simulation [6–9], quantum sensing [10,11], magnetometry [12,13], timekeeping [14,15], quantum networks [16,17], and tests on the foundational principle of quantum mechanics [18]. However, the preparation of such correlated quantum states typically requires an extremely high degree of control of the individual state of the atoms, which has been the primary experimental challenge for realizing quantum technologies. Generally, the roadmap towards realizing large-scale quantum systems is to first develop the technology to a high level such that high fidelities are achieved, then use quantum error correction to overcome the remaining errors [19,20].

An example of such a many-body entangled state is the supersinglet state [21]. Supersinglets are defined as states of total spin zero, consisting of  $N$  spin- $j$  particles. Supersinglets have the property that they are invariant under arbitrary total spin rotations. The variance of the total spin in any basis is also zero, hence they are an example of a state with zero quantum noise, suggesting uses in quantum metrology. The simplest example of a supersinglet is the  $N = 2$  spin-1/2 case, with wave function  $(|0\rangle|1\rangle - |1\rangle|0\rangle)/\sqrt{2}$ . They are typically highly entangled states, and have been proposed for a wide variety of applications such as cryptography [21], clock synchronization [14,15], quantum metrology [22], quantum teleportation [23–25], quantum computing [26,27], and decoherence free subspaces [22] and play a fundamental role in performing entanglement purification [28].

There have been several demonstrations and proposals to experimentally generate supersinglets. One approach has been to use quantum nondemolition (QND) measurements of atomic ensembles containing  $N \approx 10^6$  atoms to produce a macroscopic singlet state of the atoms [22,29–31]. Behbood *et al.* used stroboscopic QND measurements along different spin axes to generate a collective singlet state of the hyperfine ground states of  $^{87}\text{Rb}$  [30]. This approach has been applied

\*tim.byrnes@nyu.edu

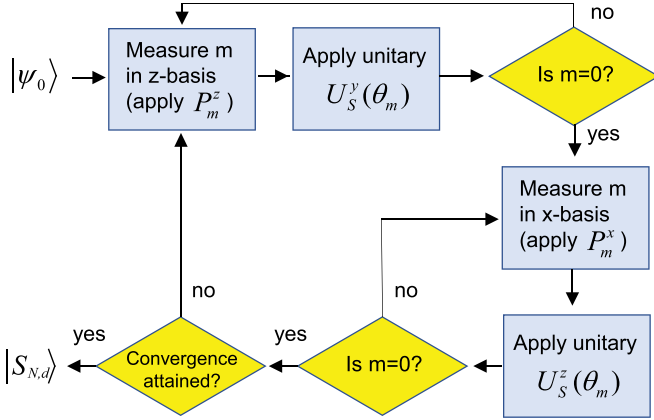


FIG. 1. The procedure considered in this paper to generate supersinglets. Starting from an arbitrary initial state  $|\psi_0\rangle$ , the repeat-until-success projection sequence (27) is first applied in the  $z$  basis. Once an  $m = 0$  is obtained, a similar sequence is performed in the  $x$  basis (31). These two sequences are repeated until convergence is attained. Convergence is defined as repeated  $m = 0$  outcomes for both the  $z$ - and  $x$ -basis projections.

to both cold atoms [30] and a hot interacting atomic gas [31]. In another work, Behbood *et al.* incorporated a feedback mechanism between the stroboscopic QND measurements to provide corrections or adjustments to the quantum state of the atoms based on information from the previous measurement outcome [29]. Typically, postselection is used to infer the presence of a macroscopic singlet state at the end of measurements [29–31]. These experiments were based upon the theoretical proposal of Ref. [22], where it was shown that QND measurements can produce squeezing towards a supersingletlike state. However, even in this theoretical work, it was not shown that a perfect supersinglet state could be attained even in the ideal case, with only squeezing of spin variables being calculated. For smaller  $N$ , several methods have been proposed to generate supersinglets using approaches such as cavity quantum electrodynamics [32–35].

In this paper, we present a scheme that deterministically generates a supersinglet state. In our scheme, a projective measurement is performed on the collective spin of the particles in the  $z$  basis, recording the total spin projection. A local rotation is then performed on half the atoms selected at random conditional on the measurement result. This increases the singlet state admixture, thereby building coherence between the quantum states. This process is repeated until the zero spin outcome is obtained. Then the process is repeated in the  $x$  basis, again until a zero spin outcome is obtained. Repeating this sequence of measurements allows for convergence to a supersinglet state (see Fig. 1 for the sequence). An important feature of the scheme is that it works for an arbitrary initial state, and no postselection is required. The key reason for this is that our sequence has the zero spin state as a unique fixed point and the system keeps evolving until it reaches this state. Our main proposal is generic and can be performed in principle on any physical system. We show an example implementation based on QND measurements of atomic ensembles.

This paper is organized as follows. In Sec. II we briefly review the physical system and the required operations to realize our procedure. In this section we also show how QND measurements could be used to realize the projective measurements in an ensemble of atoms. In Sec. III we give the detailed procedure used for the deterministic preparation of supersinglets, and the associated mathematical formalism. In Sec. IV we demonstrate that our procedure works by performing several numerical simulations. Finally the summary and conclusions are presented in Sec. V.

## II. COLLECTIVE SPIN MEASUREMENTS AND ROTATIONS

### A. The physical system

We first describe the types of operations that will be required in order to realize the supersinglets. Consider a collection of  $N$  particles of spin  $j$ . We may construct a basis for the  $(2j + 1)^N$  Hilbert space using the vectors

$$|m_1, \dots, m_N\rangle = \bigotimes_{n=1}^N |j, m_n\rangle. \quad (1)$$

Spin operators on the  $n$ th and  $m$ th particle satisfy commutation relations

$$[J_n^\alpha, J_m^\beta] = i\delta_{nm}\epsilon_{\alpha\beta\gamma}J_n^\gamma, \quad (2)$$

where  $\epsilon_{\alpha\beta\gamma}$  is the Levi-Civita antisymmetric tensor and  $\alpha, \beta, \gamma \in \{x, y, z\}$ . The states on the  $n$ th particle are eigenstates of the operator

$$J_n^z|j, m_n\rangle = m_n|j, m_n\rangle. \quad (3)$$

Here  $m_n \in \{-j, \dots, j\}$  is the  $z$ -projection spin quantum number for the  $n$ th particle.

It is also possible to construct a basis using collective spin states. Define the collective spin operators

$$J^\alpha = \sum_{n=1}^N J_n^\alpha, \quad (4)$$

again for  $\alpha \in \{x, y, z\}$ . The  $z$ -projection collective spin has eigenstates

$$J^z|J, d, m\rangle = m|J, d, m\rangle, \quad (5)$$

and the total spin squared operator (Casimir invariant)

$$J^2 = (J^x)^2 + (J^y)^2 + (J^z)^2, \quad (6)$$

which has the eigenvalue relation

$$J^2|J, d, m\rangle = J(J + 1)|J, d, m\rangle. \quad (7)$$

Here  $d$  is a label for each distinct  $J$  multiplet [36]. For example, when adding three  $j = 1/2$  spins, there are two ways of obtaining  $J = 1/2$ . The number of orthogonal basis elements is the same in the collective picture, such that

$$\sum_{J=J_{\min}}^{J_{\max}} \sum_{d=1}^{D_J} \sum_{m=-J}^J 1 = (2j + 1)^N, \quad (8)$$

where we denoted the number of distinct  $J$  multiplets as  $D_J$ . The minimum and maximum value of the collective spins are  $J_{\min} = (N \bmod 2)j$  and  $J_{\max} = Nj$ .

Supersinglet states are then defined as states in the zero total spin sector:

$$|S_{N,d}\rangle = |J = 0, d, m = 0\rangle. \quad (9)$$

Properties and applications of supersinglets may be found in Ref. [21].

### B. Required controls

We now describe the types of quantum operations that will be required for the procedure that we introduce in Sec. III.

The first capability that we will require is the ability to perform collective spin projections. Specifically, we assume that it is possible to perform the projective operator

$$P_m^z = \sum_{J=J_{\min}}^{J_{\max}} \sum_{d=1}^{D_J} |J, d, m\rangle \langle J, d, m|, \quad (10)$$

where the superscript  $z$  denotes the basis of the spin states involved in the projector. This projection operator can also be written in the individual spin basis:

$$P_m^z = \sum_{\sum_{n=1}^N m_n = m} |m_1, \dots, m_N\rangle \langle m_1, \dots, m_N|. \quad (11)$$

A second capability that we assume is to perform unitary rotations on either part or all of the spins. Define the collective spin operator for a subensemble of the spins as

$$J_S^\alpha = \sum_{n \in S} J_n^\alpha \quad (12)$$

where  $S$  specifies which spins are in the subensemble and  $\alpha \in \{x, y, z\}$ . The unitary rotation for the subensemble is then

$$U_S^\alpha(\theta) = e^{-iJ_S^\alpha \theta}. \quad (13)$$

For a unitary rotation on the whole ensemble, our notation is to omit the subensemble label:

$$U^\alpha(\theta) = e^{-iJ^\alpha \theta}. \quad (14)$$

Using this unitary operator, we may define projections along other axes. In particular we will also use projections along the  $x$  axis, defined as

$$P_m^x = U^y(\pi/2) P_m^z [U^y(\pi/2)]^\dagger. \quad (15)$$

In this way, combining  $z$ -axis measurements with unitary rotations [37–39] allows for the coherence between atomic levels to be measured.

### C. Example implementation: Atomic ensembles

A variety of physical systems could potentially be used to implement the operations that were introduced in the previous section. We now give a specific physical implementation of how the projective operator can be achieved in atomic ensembles with QND measurements.

We consider an atomic ensemble containing  $N$  atoms, where the hyperfine ground states can be used to store quantum information. A typical example would be  $^{87}\text{Rb}$ , where only the ground-state levels  $F = 1$ ,  $m_F = -1$  and  $F = 2$ ,  $m_F = 1$  are populated [40,41]. The ground states have a long coherence time due to the lack of spontaneous emission.

In this case, each atom can be considered a  $j = 1/2$  spin, and the atomic ensemble as a whole forms a collective spin. Either hot or cold atomic ensembles can be used, but a Bose-Einstein condensate cannot be used in this case because the atoms should be distinguishable such that a supersinglet is available. For degenerate atoms, the atoms form only the maximal total spin, and a supersinglet state does not exist.

A projective measurement of the form (10) can be realized using QND measurements. QND measurements have been used extensively as a means to perform measurements on atomic systems, and have been used as a way of generating entangled states [42–49]. In particular, one of the important applications in atoms is as a method of creating squeezed states [50–56] in atomic ensembles. In this approach, the light acquires an atomic state-dependent phase shift, which is then interfered after passing through the atoms. The technique has been used to propose a scheme for entangling two spatially separated atomic condensates [57] and realizing non-Gaussian correlated states such as macroscopic Schrödinger cat states [58] in atomic condensates. For atomic ensembles, information about the state of the atoms is acquired by the light pulse nondestructively, and may be used to further manipulate the state of the atom *in situ*.

Several works have already provided a theory of QND measurements, and here we give a brief description of the formalism. We use the exact wave-function approach developed in Refs. [48,49] to describe dispersive imaging measurements. The basic idea is to interact the atomic ensemble with an optical coherent state via the QND Hamiltonian [48,59]

$$\hat{H} = \hbar g J^z \hat{n}, \quad (16)$$

where  $g$  is the atom-light coupling frequency,  $\hat{n} = a^\dagger a$  is the photon number operator of the light, and  $a$  is a bosonic annihilation operator for the photons. Such an interaction entangles the light and the atoms. Performing a measurement on the light in a suitable basis, this collapses the wave function such that an indirect measurement of the atoms is made.

Specifically, consider an optical coherent state  $|\gamma\rangle$  that interacts with some arbitrary initial state of the atoms

$$|\Psi_0\rangle = \sum_{J=J_{\min}}^{J_{\max}} \sum_{d=1}^{D_J} \sum_{m=-J}^J \psi_{Jdm} |J, d, m\rangle \quad (17)$$

according to the Hamiltonian (16) for a time  $t$ . If the light then interferes with another coherent state of light  $|\chi\rangle$  via a beamsplitter and photon detection is performed, then the final un-normalized state can be calculated to be after a Gaussian approximation [49,58]

$$\begin{aligned} |\Psi_{n_c, n_d}\rangle &= \frac{e^{\frac{n_c + n_d - |\gamma|^2 - |\chi|^2}{2}}}{(4\pi^2 n_c n_d)^{\frac{1}{4}}} \left( \frac{|\gamma|^2 + |\chi|^2}{n_c + n_d} \right)^{\frac{n_c + n_d}{2}} \\ &\times e^{-i\frac{\pi}{2} n_d} \sum_{J=J_{\min}}^{J_{\max}} \sum_{d=1}^{D_J} \sum_{m=-J}^J e^{i(n_c + n_d)(\phi - gtm)} \\ &\times e^{i(n_c \phi_c + n_d \phi_d)} e^{-\frac{1}{2\sigma^2} (m - m_0)^2} \psi_{Jdm} |J, d, m\rangle, \quad (18) \end{aligned}$$

where  $n_c$  and  $n_d$  are the photon counts for the two modes after interference of the optical modes. The probability of this outcome is given by  $P_{n_c, n_d} = \langle \Psi_{n_c, n_d} | \Psi_{n_c, n_d} \rangle$  and is the probability

of obtaining  $n_c$  and  $n_d$  photons in the measurement. Here we defined phases as

$$\begin{aligned}\phi &= \frac{gtm}{2} + \frac{\arg(\chi) - \arg(\gamma)}{2} + \frac{\pi}{4} + \frac{\phi_p}{2}, \\ \phi_c &= \arctan(\tan \eta \tan \phi), \\ \phi_d &= \arctan\left(\frac{\tan \phi}{\tan \eta}\right).\end{aligned}\quad (19)$$

The phase  $\phi_p$  is a phase offset. We defined  $\eta$  as the ratio of the amplitude of the light coherent state:

$$\tan \eta = \frac{|\chi| - |\gamma|}{|\chi| + |\gamma|}.\quad (20)$$

The Gaussian factor in (18) makes it clear that the effect of the QND measurements is to modify the amplitudes of the coefficients such that they are concentrated near the maximum value:

$$m_0 = \frac{1}{gt} \left[ \arcsin\left(\frac{1}{\cos 2\eta} \frac{n_d - n_c}{n_d + n_c}\right) - \arg(\chi) + \arg(\gamma) - \phi_p \right].\quad (21)$$

The variance of the Gaussian is meanwhile

$$\sigma^2 = \left( \frac{g^2 t^2}{8} \frac{n_c + n_d}{n_c n_d} [(n_c + n_d)^2 \cos^2 2\eta - (n_c - n_d)^2] \right)^{-1}.\quad (22)$$

The variance of the Gaussian determines whether the measurement that is made is either a strong projective measurement or a weak measurement. If  $\sigma$  is large, then the original wave function (17) is only slightly modulated, and produces number state squeezing. In the strong measurement regime,  $\sigma$  is small, with only a few states having nonzero amplitude in the vicinity of  $m = m_0$ . In the extreme case, characterized by  $|\chi|, |\gamma| \gg 1$ , only one of the probability amplitudes near  $m_0$  is nonzero [60]. This limit of QND measurements acting as a strong projective measurement can be used to realize (10).

The unitary rotations on half the atoms in the ensemble can be realized using optical Raman pulses illuminating half the spatial region of the atomic ensemble. In order to only rotate half the atoms in the ensemble, the operation should complete before the atoms move out of the spatial region that illuminates the ensemble. For a hot atomic ensemble in a cell of size  $\approx 1$  cm, the velocities of the atoms are typically  $\approx 300$  m/s. This gives a time window of  $\approx 17$   $\mu$ s, easily accessible using current techniques of Raman pulses. Furthermore, composite pulses [61] could be used to enhance the fidelity of the rotations in presence of various inhomogeneities in the atomic ensemble.

### III. PROCEDURE FOR DETERMINISTIC PREPARATION OF SUPERSINGLET STATES

We now describe the procedure using the projective measurements and unitary rotations of Sec. II B to prepare the supersinglet states.

#### A. The basic idea

Given an arbitrary initial state  $\rho_0$ , we would like to have a procedure that deterministically gives us the supersinglet

state  $|S_{N,d}\rangle$ , using only the collective operations as given in Sec. II B. Depending upon the particle number  $N$ , there may be more than one distinct supersinglet state. For our purposes, any superposition or mixture of such supersinglet states will suffice. The important aspect will be that the total spin  $J$  is zero. We note that in order to have a supersinglet state, we require  $N$  to be an even number. For the procedure that we introduce here, we will assume  $N$  is even. Later we examine the effect of odd  $N$  in Sec. IV E.

The key insight that yields our procedure is the fact that a supersinglet state is invariant under rotations. That is,

$$e^{-i(\theta_x J^x + \theta_y J^y + \theta_z J^z)} |S_{N,d}\rangle = |S_{N,d}\rangle\quad (23)$$

up to a global phase and  $\theta_\alpha$  are arbitrary coefficients. This means that it is an eigenstate of both projection operators  $P_0^z$  and  $P_0^x$ , such that

$$\begin{aligned}P_0^z |S_{N,d}\rangle &= |S_{N,d}\rangle, \\ P_0^x |S_{N,d}\rangle &= |S_{N,d}\rangle.\end{aligned}\quad (24)$$

It follows that if one were to start in the singlet state, the sequence of  $2M$  projections made alternately in the  $x$  and  $z$  basis would be invariant:

$$(P_0^x P_0^z)^M |S_{N,d}\rangle = |S_{N,d}\rangle.\quad (25)$$

Regarded as a measurement sequence, the probability of this outcome is 1, since the state does not lose any amplitude after the projection. This invariance under projections in different bases is one of the key ingredients of our procedure. Other states with  $J \neq 0$  become rotated with each change of basis and do not have the invariance property of (25).

Starting from an arbitrary state  $|\psi\rangle$ , performing a projection in the  $z$  basis gives a probability of getting an outcome  $m$  according to

$$p_m = \langle \psi | P_m^z | \psi \rangle.\quad (26)$$

Of course in general there is no guarantee that we will obtain the  $m = 0$  outcome as in (25). To overcome this, we perform a conditional unitary rotation after each projection, such as to maximize the probability of getting the desired  $m = 0$  outcome [22]. Once the  $m = 0$  outcome is obtained, the next set of projections in the  $x$  basis is performed, where the procedure is repeated, until the  $m = 0$  outcome is obtained. Repeating this procedure creates a sequence such that a singlet state is deterministically produced (Fig. 1).

#### B. The procedure

We now rephrase the procedure introduced in the previous section mathematically to make it more precise. We first define the repeat-until-success projection sequence as

$$\begin{aligned}\mathcal{P}_m^z &= \prod_{l=1}^L [U_S^y(\theta_{m_l}) P_{m_l}^z] \\ &= P_0^z U_S^y(\theta_{m_{L-1}}) P_{m_{L-1}}^z \cdots U_S^y(\theta_{m_1}) P_{m_1}^z\end{aligned}\quad (27)$$

where the product symbol multiplies the matrices in reverse order, i.e., from  $l = 1$  to  $L$  from right to left. The unitary rotation is applied on the set  $\mathcal{S}$  involving half of the spins.

The record of all the measurement outcomes is specified by

$$\vec{m} = (m_1, m_2, \dots, m_L). \quad (28)$$

In the sequence (27),  $L$  is taken large enough that the  $m = 0$  outcome is obtained on the  $L$ th projection. For all  $l \in [1, L - 1]$ ,  $m_l \neq 0$ . For this reason, the final projection always takes the value  $m_L = 0$ , and the final unitary rotation is simply the identity matrix.

The angles  $\theta_m$  are chosen such as to maximize the probability of getting a  $m = 0$  outcome on the subsequent projection. That is, the state after a projection to spin  $m$  is rotated to

$$U_S^y(\theta_m)|J, d, m\rangle = \sum_{J'd'm'} |J', d', m'\rangle \times \langle J', d', m' | U_S^y(\theta_m) | J, d, m \rangle. \quad (29)$$

The rotation operation repopulates other Dicke states by putting them in linear superposition. A suitable choice for the rotation angle is obtained by making the magnitude of the matrix element for  $m' = 0$  large, which we take to be

$$\theta_m = \arcsin\left(\frac{m}{\sqrt{J_{\max}(J_{\max} + 1)}}\right). \quad (30)$$

For  $m = 0$ ,  $\theta_m = 0$  and the rotation operation is the identity matrix. It is important that the rotation is performed only on half the spins as otherwise the rotation (29) is not able to change  $J$ , i.e., only  $J' = J$  are nonzero in the matrix elements. Since our aim is to obtain the singlet state  $J = 0$ , the ability to change  $J$  is obviously crucial to the operation. Which spins are chosen do not particularly matter for the procedure, and they may be chosen at random.

Once the desired  $m = 0$  outcome is obtained, another repeat-until-success projection sequence is applied, this time in the  $x$  basis:

$$\begin{aligned} \mathcal{P}_{\vec{m}}^x &= \prod_{l=1}^L [U_S^z(\theta_{m_l}) P_{m_l}^x] \\ &= P_0^x U_S^z(\theta_{m_{L-1}}) P_{m_{L-1}}^x \dots U_S^z(\theta_{m_1}) P_{m_1}^x. \end{aligned} \quad (31)$$

Again, the unitary operations are designed such that the probability of obtaining  $m = 0$  on the next measurement is maximized.

The final sequence that we propose in the pure states formalism is (see Fig. 1)

$$\prod_{k=1}^{K-1} (\mathcal{P}_{\vec{m}_{2k}}^x \mathcal{P}_{\vec{m}_{2k-1}}^z) |\psi_0\rangle \rightarrow \sum_d \psi_d |S_{N,d}\rangle. \quad (32)$$

Here  $\vec{m}_l$  is the measurement sequence for the  $l$ th round of measurements. The two measurement sequences are repeated many times until measurement convergence is attained. Once the singlet state is obtained, no unitary rotation is necessary and projectors in both the  $z$  and  $x$  bases give  $m = 0$ , as in (25). We define convergence being attained when the projection sequence such as in (25) consecutively returns  $m = 0$  for several measurements. Our claim is that such a sequence always converges to a singlet state, from an arbitrary initial state  $|\psi_0\rangle$ . On the right-hand side of (32) we have written an arbitrary superposition with coefficients  $\psi_d$  of the distinct supersinglet states. As we shall see, our procedure is sensitive

only to whether the state is a supersinglet state or not, and does not distinguish between the distinct supersinglet states.

We may also write (32) for the mixed state case:

$$\begin{aligned} & \left[ \prod_{k=1}^{K-1} (\mathcal{P}_{\vec{m}_{2k}}^x \mathcal{P}_{\vec{m}_{2k-1}}^z) \right] \rho_0 \left[ \prod_{k=1}^{K-1} (\mathcal{P}_{\vec{m}_{2k}}^x \mathcal{P}_{\vec{m}_{2k-1}}^z) \right]^\dagger \\ &= \mathcal{P}_{\vec{m}_{2K}}^x \mathcal{P}_{\vec{m}_{2K-1}}^z \dots \mathcal{P}_{\vec{m}_2}^x \mathcal{P}_{\vec{m}_1}^z \rho_0 \mathcal{P}_{\vec{m}_1}^z \mathcal{P}_{\vec{m}_2}^x \dots \mathcal{P}_{\vec{m}_{2K-1}}^z \mathcal{P}_{\vec{m}_{2K}}^x \\ &\rightarrow \sum_{dd'} \rho_{dd'} |S_{N,d}\rangle \langle S_{N,d'}|. \end{aligned} \quad (33)$$

Again, our procedure deterministically generates an arbitrary mixture or superposition of supersinglet states, hence we have written these coefficients as  $\rho_{dd'}$ .

We note that our procedure can be viewed as an adaptation of the imaginary time evolution procedure as presented in Ref. [62]. In Ref. [62], a procedure was introduced to target the ground state of a given Hamiltonian. The procedure involves a sequence of measurements and conditional unitary rotations, chosen in such a way that the target state is a fixed point of the evolution. This same structure is apparent in the repeat-until-success projection sequence (27) and (31). The singlet state is a fixed point of the total sequence as given in (32), where eventually the sequence converges to only  $m = 0$  outcomes as in (25).

## IV. NUMERICAL EVOLUTION

We now illustrate the singlet state preparation procedure given in Sec. III by performing a numerical evolution of various cases.

### A. Simulation details

The initial state that we will use in most of our numerical evolutions is a completely mixed state:

$$\rho_0 = \frac{\mathbb{1}^{\otimes N}}{2^N}. \quad (34)$$

This state can be viewed equivalently as a thermal state at infinite temperature. This same initial state was used in works such as Ref. [30] to experimentally target a singlet state. Although the supersinglet state can always be generated from an arbitrary initial state in our procedure, we shall use the completely mixed state as our initial state since it is a state that possesses no entanglement or coherence [63,64]. Since a supersinglet state possesses both entanglement and coherence, convergence towards the supersinglet state shows that our procedure is responsible for creating these quantum properties.

The evolution sequence is performed by taking the initial state (34) in the procedure (33). Each projection operation is chosen randomly according to Born probabilities. We perform this with an accept-reject procedure as given in the Appendix. Due to the randomness of measurements, each run of the procedure gives a different evolution. The atoms to which the unitary rotations (13) are performed are chosen randomly each time the unitary operation is applied, selecting half the spins at random. The measurement sequence is performed multiple times, for which we check for the convergence to the singlet state. We consider convergence to be attained if five

consecutive measurements in alternating  $z$  and  $x$  bases give the  $m = 0$  outcome.

To characterize the state obtained after a measurement in the sequence, we will evaluate several quantities. The first is the normalized average value of the total spin squared as given in (6):

$$\begin{aligned} \bar{J}^2 &\equiv \frac{\langle J^2 \rangle}{J_{\max}(J_{\max} + 1)} \\ &= 0 \quad (\text{singlet}). \end{aligned} \quad (35)$$

The above quantity has an expectation value of zero for a singlet state since the eigenvalue of the Casimir invariant is  $J(J + 1)$ . This quantity lies in the interval  $0 \leq \bar{J}^2 \leq 1$  due to the normalization factor. Only the singlet states have a zero expectation value for this operator and hence it is a good detector for the supersinglet state. The expectation value of  $J^2$  is nonzero for the thermal state since it involves contributions from total spin sectors  $J > 0$ . For the first-order spin expectation values, both the initial thermal state (34) and the singlet state have zero expectation values:

$$\langle J^\alpha \rangle = 0, \quad (\text{singlet and completely mixed}) \quad (36)$$

for  $\alpha \in \{x, y, z\}$ . Hence the variance of the spins for a singlet state will be zero:

$$\begin{aligned} (\Delta J^\alpha)^2 &\equiv \langle (J^\alpha)^2 \rangle - \langle J^\alpha \rangle^2 \\ &= 0 \quad (\text{singlet}). \end{aligned} \quad (37)$$

This also shows the squeezed nature of the spin observables for the singlet state. The other way we will quantify the state is using fidelity, defined as

$$F = \sum_d F_d, \quad (38)$$

$$F_d = \langle S_{N,d} | \rho | S_{N,d} \rangle, \quad (39)$$

where  $\rho$  is the state at a particular point in the projection sequence. This is a useful measure to show the exact state that has been reached in the procedure, whereas (35) does not distinguish between distinct supersinglets.  $F = 1$  indicates that the state  $\rho$  is a singlet state, with  $F_d$  showing the decompositions.

### B. $N = 4$ case

We first consider a relatively small system consisting of  $N = 4$  spins, each with  $j = 1/2$ . This example will illustrate some of the basic properties of the supersinglet state preparation procedure. For this and the next section we shall only consider the even  $N$  case, and discuss the odd  $N$  case in Sec. IV E.

The  $N = 4$  case is the smallest system that illustrates that the supersinglet state is not a unique state, due to angular momentum addition. There are two distinct supersinglet states [36] for four  $j = 1/2$  spins, given by [21]

$$|S_{4,1}\rangle = \frac{1}{\sqrt{3}}[|\phi_+\rangle^{\otimes 2} - |\phi_-\rangle^{\otimes 2} - |\psi_+\rangle^{\otimes 2}], \quad (40)$$

$$|S_{4,2}\rangle = |\psi_-\rangle^{\otimes 2}, \quad (41)$$

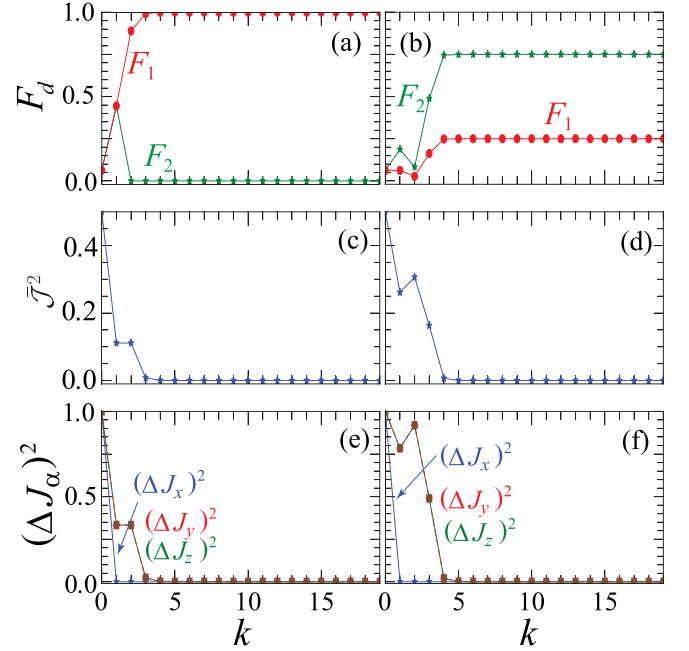


FIG. 2. Evolution according to the procedure (33) for  $N = 4$  spin  $j = 1/2$  particles for an initial state being a completely mixed state (34). The horizontal axis shows the number of rounds of  $z$ - and  $x$ -basis measurement sequences, i.e., the variable  $k$  in (32). Two different trajectories are shown: for each run the (a), (b) fidelity (39), (c), (d) normalized total spin squared (35), and (e), (f) spin variances (37) are shown. Lines connecting the markers are to guide the eye. All plotted quantities are dimensionless.

where we defined the Bell states for two  $j = 1/2$  spins as

$$\begin{aligned} |\phi_{\pm}\rangle &= \frac{1}{\sqrt{2}}(|+\rangle|+\rangle \pm |-\rangle|-\rangle), \\ |\psi_{\pm}\rangle &= \frac{1}{\sqrt{2}}(|+\rangle|-\rangle \pm |-\rangle|+\rangle). \end{aligned} \quad (42)$$

Here the  $N = 2$  singlet state is  $|\psi_-\rangle$  and the remaining three states form a  $J = 1$  triplet. The first  $N = 4$  supersinglet (40) is given as a linear combination of the triplet states, while the second supersinglet (41) is simply two  $N = 2$  singlet states. Any linear combination or mixture of the two distinct supersinglet states is also a supersinglet state. The supersinglet state is invariant under rotations of the total spin, as given in (23).

Our numerical results are presented in Fig. 2 for two sample evolutions. We observe from the fidelity and the total spin squared that the supersinglet state is reached after approximately four rounds of projections. The two evolutions that we show are merely examples. We have run our procedure for over 1000 trajectories and found that in 100% of the cases the supersinglet state is reached. The number of projections within each repeat-until-success projection sequence decreases with the number of rounds, with the largest number being in the first round  $k = 1$ . A typical number of measurements in the first round is an order of ten  $z$  measurements or  $x$  measurements. While a supersinglet state is always reached with  $F = 1$ , Figs. 2(a) and 2(b) reveal that the final contributions to the two distinct supersinglets are not always

the same. We observe that each time the fidelity  $F_1 > F_2$ , eventually the state approaches the state  $|S_{4,1}\rangle$ . On the hand, whenever  $F_2 > F_1$ , the fidelities converge towards  $F_1 = 0.25$  and  $F_2 = 0.75$ .

All spin variances start out being unity corresponding to their value for a completely mixed state. After one round of measurements, the final projection that is made is  $P_0^x$ . Hence the state of the system after one round of measurements is always an eigenstate of the  $J^x$  operator. For this reason, the error of the state for all  $k > 0$  has zero variance for  $J^x$  as seen in Figs. 2(e) and 2(f). The variances for the other spin directions are still typically nonzero at this point at  $k = 1$ . For each sequence, the measurement outcomes are random, hence the evolution of the variance evolves towards zero along different trajectories. Another source of randomness is the random selection of the spins to be rotated in the conditional unitary rotations. As the state settles into a supersinglet state, the error along the  $y$  axis and  $z$  axis becomes zero, as seen in Figs. 2(e) and 2(f), heralding the realization of a supersinglet state.

### C. Spin-polarized initial state

Our procedure to generate the supersinglet state is invariant to initial conditions. To show this, we now repeat the calculations for  $N = 4$  and  $j = 1/2$ , but starting in a spin coherent state [65]. We consider in particular the state polarized in the  $y$  direction:

$$|\psi_0\rangle = e^{-iJ^x\pi/2}|J, d = 1, m = J\rangle. \quad (43)$$

Here  $|J, d = 1, m = J\rangle$  is the Dicke state polarized in the  $z$  direction. Rotating this around the  $x$  axis by an angle  $\pi/2$  gives a  $y$ -polarized state. We choose a  $y$ -polarized state since we perform projections in the  $x$  and  $z$  basis, and this produces a large backaction in either case.

Our numerical results are shown in Fig. 3 for two example evolutions. We see a similar behavior to the results obtained in Fig. 2. We observe from the fidelity and the total spin squared that the supersinglet state is reached after approximately five rounds of projections. While a supersinglet state is always reached with  $F = 1$ , Figs. 3(a) and 3(b) reveal that the final contributions to the two distinct supersinglets are not always the same. Again the same pattern of convergence to either  $F_1 = 0.25$ ,  $F_2 = 0.75$  or  $F_1 = 1$ ,  $F_2 = 0$  is seen as with the previous case. For the variances, since the initial state is polarized along the  $y$  axis, the  $J^y$  spin variance starts out being zero, and the variances of  $J^x$  and  $J^z$  start out being unity. After one round of measurements, the final projection that is made is  $P_0^x$ . For this reason, the error of the state for all  $k > 0$  has zero variance for  $J^x$  as seen in Figs. 3(e) and 3(f). The variance of  $J^y$  increases after the first measurement to the same value as the variance of  $J^z$ , due to the effect of backaction. As the state settles into a supersinglet state, the error along the  $y$  axis and  $z$  axis becomes zero, as seen in Figs. 2(e) and 2(f).

### D. Larger number of spins

We now repeat the calculation for a larger number of spins. We consider  $N$  spin-1/2 particles, where we take  $N$  even. Due to the necessity to simulate the full Hilbert space

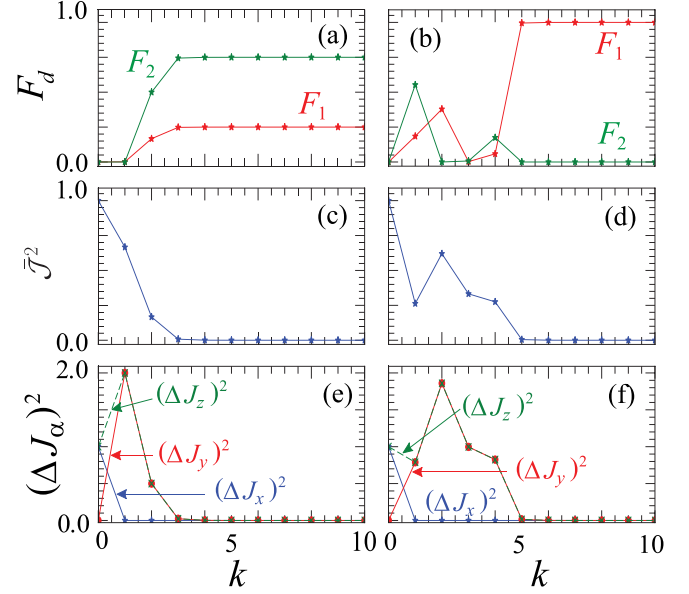


FIG. 3. Evolution according to the procedure (33) for  $N = 4$  spin  $j = 1/2$  particles with an initial state being a  $y$ -polarized spin coherent state (43). The horizontal axis shows the number of rounds of  $z$ - and  $x$ -basis measurement sequences, i.e., the variable  $k$  in (32). Two different runs are shown: For each run the (a), (b) fidelity (39), (c), (d) normalized total spin squared (35), and (e), (f) spin variances (37) are shown. Lines connecting the markers are to guide the eye. All plotted quantities are dimensionless.

of dimension  $2^N$  the largest system that we could simulate within a reasonable time was  $N = 10$ . The major numerical overhead results in evaluating matrix multiplications due to the unitary transformations, which have a dimension  $2^N \times 2^N$ . For this case, we will only calculate the expectation values and variances of the spin operators, since there are a larger number of distinct singlet states. In this case there are a total of 42 distinct singlet states [36]. We follow the procedure as given in Sec. IV A, again starting from a completely mixed state.

The results are shown in Fig. 4. As for the smaller system size considered before, the state converges towards a supersinglet state, as can be seen from the total spin squared operator. Remarkably, the convergence is attained with a similar number of rounds of measurement sequences, typically after about  $k = 5$  full convergence was attained. The number of projections within a single projection sequence was larger; the number of measurements in a single sequence (27) and (31) was typically of the order of 100  $z$  measurements and  $x$  measurements. It is to be expected that a larger number of projections are necessary for a larger system size, due to the larger Hilbert space that the state must traverse during the evolution. It is nevertheless remarkable that such fast convergence is attained for a significantly larger system.

For the variances, we again see fast convergence towards zero variance for all spin directions. As was the case for the smaller system, some random fluctuations are seen during the evolution, where occasionally the variance increases. However, within approximately five rounds variances decay to zero.

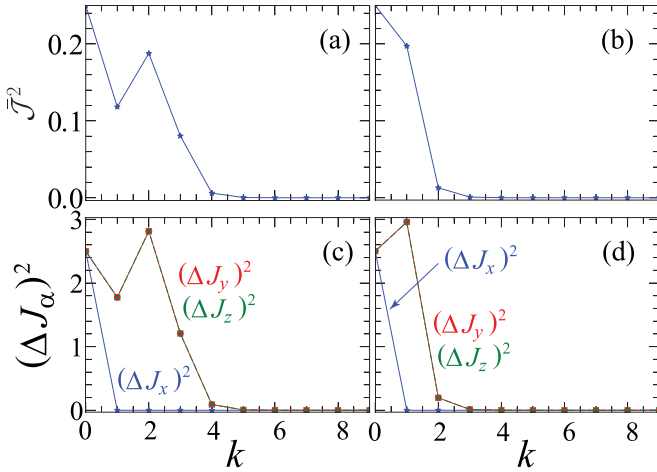


FIG. 4. Evolution according to the procedure (33) for  $N = 10$  spin  $j = 1/2$  particles. The horizontal axis shows the number of rounds of  $z$ - and  $x$ -basis measurement sequences, i.e., the variable  $k$  in (32). The initial state is set as the completely mixed state (34). Two different runs are shown: for each run the (a, b) normalized total spin squared (35) and (c), (d) spin variances (37) are shown. Lines connecting the markers are to guide the eye. All plotted quantities are dimensionless.

### E. Odd number of spins

Depending upon the experimental realization, the number of spins  $N$  may not be a precisely controllable quantity. This is true of the atomic ensemble implementation that is suggested in Sec. II C, where the number of atoms is typically very large and not controlled at the single atom level. A potential problem arises here because for odd  $N$  a supersinglet state does not exist. For example, the smallest total spin that can be realized for an odd number of  $j = 1/2$  spins is a total spin of  $J = 1/2$ . We show in this section how such a scenario can be handled, and how convergence can still be attained towards a small total spin.

To handle this case, we follow the same procedure as given in Fig. 1, except that we replace the criterion for exiting the repeat-until-success projection sequence to  $|m| \leq m_{\text{cut}}$ . Hence for targeting a genuine singlet state we have  $m_{\text{cut}} = 0$ , but for the odd  $N$  case we set  $m_{\text{cut}} = 1/2$ , since  $m = 0$  does not exist. This cutoff introduces a wider variety of states that the sequence can potentially converge to. This makes the convergence in the repeat-until-success projection sequence typically faster, since there are more states that are allowable in the criterion. However, there is a tradeoff as a larger  $m_{\text{cut}}$  reduces the fidelity with respect to the desired target state.  $m_{\text{cut}}$  can be viewed as an adjustable parameter that can control the convergence speed, at the expense of a less accurate target state. Having such a parameter can be useful even in the context of even  $N$ , if  $N$  is a very large number. A very large  $N$  may mean that the convergence of the repeat-until-success sequence is rather slow, but this can be mitigated by reducing the accuracy by increasing  $m_{\text{cut}}$ .

Our numerical results are shown in Fig. 5. As with the even  $N$  case considered before, the state converges towards a minimum  $J$  state, as can be seen from the total spin squared operator. The minimum state occurs for  $J = 1/2$

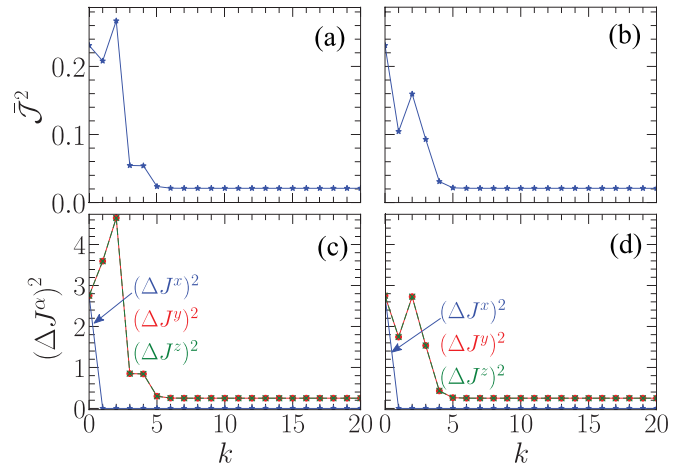


FIG. 5. Evolution according to the procedure (33) for  $N = 11$  spin  $j = 1/2$  particles. The horizontal axis shows the number of rounds of  $z$ - and  $x$ -basis measurement sequences, i.e., the variable  $k$  in (32). The initial state is set as the completely mixed state (34). Two different runs are shown: for each run the (a, b) normalized total spin squared (35) and (c), (d) spin variances (37) are shown. Lines connecting the markers are to guide the eye. All plotted quantities are dimensionless.

giving the minimum expectation value of the Casimir invariant as  $\langle J^2 \rangle = 3/4$ , which in terms of the normalized values is  $\bar{J}^2 = 3/143 \approx 0.02$ . The variance of  $J_x$  is always zero for the same reasons given previously. However, the variances of  $J_y$  and  $J_z$  settle to a minimum value of 0.25, in a departure from the even  $N$  case. Interestingly, the convergence to the minimal total spin squared state is attained with a similar number of rounds of measurement sequences as to the even  $N$  case, typically after about  $k = 5$  rounds.

### F. Measurement imperfections

One of the primary limitations of the current scheme is in the resolution of the measurements. Achieving single atom resolution has been a challenging task experimentally, although recently some progress towards this has been attained [66–68]. For QND measurements, the main limitation is the presence of spontaneous emission of the atoms and photon loss [69–71]. To produce the QND interaction, a second-order interaction involving the atomic excited states is necessary, which inevitably introduces decoherence via spontaneous emission. It was shown in Ref. [69] that for the QND scheme photon loss is a less serious problem in comparison to spontaneous emission. The basic effect of spontaneous emission is to introduce an additional dephasing effect, as is well known to occur through ac Stark shift scattering [72]. There is a dephasing effect on the light as well, which introduces noise to the photonic measurement readout. Despite these challenges, there has been tremendous progress towards measurements with precision approaching the Heisenberg limit [73,74]. This allows for the detection of the atomic population with single-atom precision. In terms of the projection operators that we consider in this paper, the measurement imperfections correspond to a false readout reading  $\tilde{m} = m + \Delta m$ , where  $\Delta m$

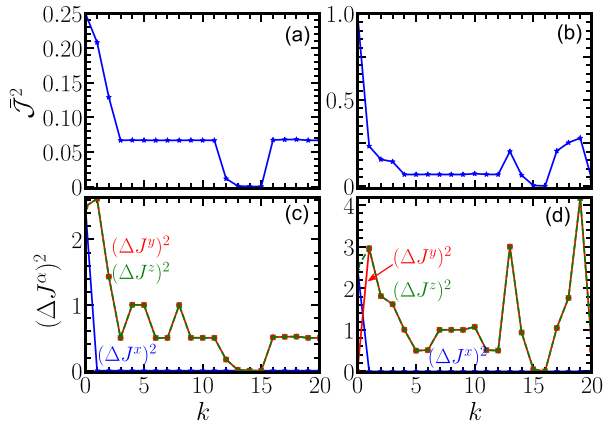


FIG. 6. Evolution according to the procedure (33) for  $N = 10$  spin  $j = 1/2$  particles in the presence of Gaussian noise. The standard deviation of the noise is taken to be  $\sigma = 1$ . The horizontal axis shows the number of rounds of  $z$ - and  $x$ -basis measurement sequences, i.e., the variable  $k$  in (32). (a) The initial state is set as the completely mixed state (34). (b) The initial state is set to a state polarized along the  $y$  direction (43). (c), (d) Spin variances corresponding to the initial states (a) and (b), respectively. Lines connecting the markers are to guide the eye. All plotted quantities are dimensionless.

is the error in the readout, when in fact a projection  $m$  has occurred.

This noise is included in our model by drawing  $\Delta m$  randomly from Gaussian noise with zero mean and standard deviation equal to  $\sigma$ ,  $\tilde{m} = m + \Delta m$ . The results are presented in Fig. 6. The results show that additional noise occurs during the convergence towards the singlet state. Compared with Fig. 4, the convergence is slower. Moreover, even if a singlet state is attained, subsequent measurements do not guarantee it to remain in the singlet state as shown in Figs. 6(a) and 6(b). Nevertheless, there is an overall reduction of the variance in comparison to the initial state. In Fig. 6 relatively small ensembles are simulated with  $\sigma = 1$ , hence the relative noise appears large. We expect that the limit of the variance is of the order of  $\sigma^2$ , which is consistent with our numerical results shown in Figs. 6(c) and 6(d).

### G. Spin-1 system

The examples up to this point considered effective spin-1/2 atoms, where only two atomic levels are populated. Here we show that this is not a necessary assumption, and provide a final example where the atoms are spin-1 particles. We consider two initial conditions, one where the spins start in a completely mixed state

$$\rho_0 = \frac{\mathbb{1}^{\otimes N}}{3^N}, \quad (44)$$

and another where the state is initially polarized along the  $y$  direction (43). The Hilbert space has a dimension  $3^N$  giving a density matrix of size  $3^N \times 3^N$ . We consider  $N = 6$  particles, which have a total of 15 supersinglet states [36]. The result of running our protocol for this case is shown in Fig. 7. The simulations rapidly converge to a supersinglet in a small

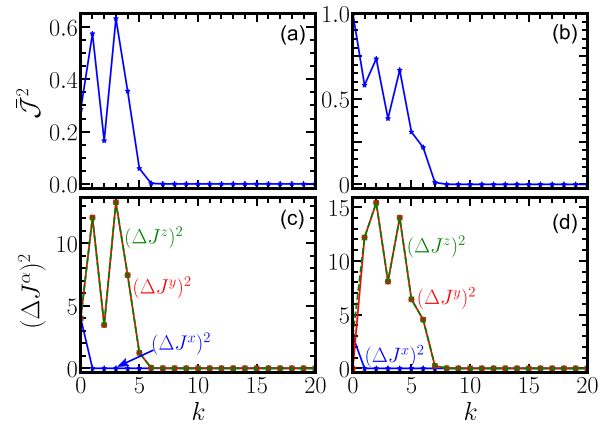


FIG. 7. Evolution according to the procedure (33) for  $N = 6$  spin  $j = 1$  particles. The horizontal axis shows the number of rounds of  $z$ - and  $x$ -basis measurement sequences, i.e., the variable  $k$  in (32). (a) The initial state is set as the completely mixed state (34). (b) The initial state is set to a state polarized along the  $y$  direction (43). (c), (d) Spin variances corresponding to the initial states (a) and (b), respectively. Lines connecting the markers are to guide the eye. All plotted quantities are dimensionless.

number of rounds, in a similar way to the  $N$  spin-1/2 particles as examined previously. The number of projections within a single projection sequence is similar to that of  $N = 10$  spin-1/2 particles, due to the similar Hilbert-space size of this example. The number of measurements in a single sequence (27) and (31) was typically of the order of 100  $z$  measurements and  $x$  measurements.

## V. SUMMARY AND CONCLUSIONS

We have proposed a scheme based on a sequence of projective measurements in the collective spin basis and conditional unitary rotations to prepare a supersinglet state. The main procedure is given in (32) and summarized in Fig. 1. The scheme deterministically produces the supersinglet state from an arbitrary initial state without postselection. Within a measurement sequence, the quantum state of the atoms collapses randomly to a state given by the projection operator. Convergence of the state towards the supersinglet is ensured by unitary rotations that repopulate the spin zero population. Using the property that a supersinglet state is invariant under total spin rotations, repeated projections in the  $z$  and  $x$  bases result in convergence to the spin zero state. The procedure is compatible for an arbitrary number of particles  $N$  and spin  $j$ .

We have found that the procedure is remarkably efficient in converging to the supersinglet state, with little difference seen in terms of the rounds of measurements required for various  $N$ . Within each measurement sequence (27) and (31) we note that it does take longer to find the  $m = 0$  outcome, which is to be expected due to the larger Hilbert space. In an atomic ensemble implementation where the atom numbers can be far larger than that simulated here (e.g.,  $N = 10^6$ ) one may worry that this will make the convergence excessively long. The number of iterations can however be alleviated by introducing tolerances to the target state. As seen in Sec. IV E it is also possible to adjust the procedure such that convergence

is towards a range of spins, and not only  $m = 0$  exactly. By setting the tolerance to the target spin sector to a larger value, one may reduce the convergence time, at the expense of a lower fidelity of the spin zero sector. In this way, the procedure should be applicable also to macroscopic systems.

We note that in contrast to existing schemes, our procedure produces the exact supersinglet state, as opposed to producing squeezing as in Ref. [22]. This can be seen in our results in Figs. 2–4 and 7, where the spin variances reduce to zero for all directions. The main reason for this is that our measurements are projective, which induces a much more dramatic effect on the state of the atoms, due to the strong measurements that affect the state. This results in a much faster convergence to the supersinglet state. Another attractive feature of our procedure is that it allows for a deterministic way of preparing the supersinglet state without involving postselection of the final state. There is also no need to prepare a special initial state. The experimental requirements only involve QND measurements which are routinely performed, and rotations on subensembles of the spins, which should be within current experimental capabilities.

We finally comment on potential applications of supersinglet states. Several applications of supersinglets have been proposed such as the liar detection test [75], secret sharing problem [32],  $N$  stranger problems [32], and encoding information in a decoherence-free subspace [21]. One issue with the supersinglet states that are generated according to our protocol is that it is insensitive to the degeneracy label  $d$ , hence one is not able to target a specific supersinglet state. Furthermore, depending on the implementation, such as with atomic ensembles where  $N$  may be extremely large, there may not be precise control with  $N$ . One potential application where such control may not be precisely necessary is quantum metrology. Here, the aim of the measurement is to detect the effect on a probe quantum state while minimizing the error. The supersinglets are invariant under rotations of the total spin, regardless of the label  $d$ . Additionally, the state of spin  $J^2 = 0$  has zero variance. Any slight deviations of the variance from zero can give information about the field. This feature may be used to sense local fields (fields that do not act on the whole ensemble or collections of atomic samples) [12]. Another potential application is in quantum clock synchronization, where the aim is to transfer timing information between distant parties. In Ref. [14], a macroscopic singlet state was used to perform this task, and it was shown in Ref. [15] that entanglement purification involving

singlet state preparation forms a crucial part to eliminate the necessity of a common phase reference. We finally mention that our protocol can be viewed as a specific implementation of measurement-based imaginary time evolution [62], where a target measurement outcome is deterministically prepared. By suitably detecting additional quantum numbers, it may be possible to further target specific states, such that particular supersinglet states are prepared.

## ACKNOWLEDGMENTS

This work is supported by the National Natural Science Foundation of China (Grant No. 62071301); NYU-ECNU Institute of Physics at NYU Shanghai; the Joint Physics Research Institute Challenge Grant; the Science and Technology Commission of Shanghai Municipality (Grant No. 19XD1423000,22ZR1444600); the NYU Shanghai Boost Fund; the China Foreign Experts Program (Grant No. G2021013002L); the NYU Shanghai Major-Grants Seed Fund; and the Talented Young Scientists Program (Grant No. NGA-16-001) supported by the Ministry of Science and Technology of China.

## APPENDIX: CHOOSING MEASUREMENT BY BORN PROBABILITIES

Each projective measurement performed in (27) and (31) must be chosen randomly according to Born probability outcomes. Here we show how we choose the measurement outcomes using an accept-reject procedure.

Suppose we wish to perform a projective measurement  $P_m|\phi\rangle$  where  $P_m$  are projectors and  $|\phi\rangle$  is an arbitrary initial state. The probability of the  $m$ th outcome is given by

$$p_m = \langle\phi|P_m|\phi\rangle \quad (\text{A1})$$

using the idempotency of projection operators. Then we may select measurement outcomes according to Born probabilities using the following algorithm.

- (1) Choose a proposed outcome  $m$  randomly from a uniform distribution.
- (2) Calculate the probability  $p_m$  according to (A1).
- (3) Choose a random real number  $r$  in the interval  $[0, 1]$  from a uniform distribution.
- (4) If  $r < p_m$  then reject and go to step 1. Otherwise accept  $m$  as the measurement outcome.

- 
- [1] P. W. Anderson, *Science* **235**, 1196 (1987).
  - [2] T. Werlang, C. Trippé, G. A. P. Ribeiro, and G. Rigolin, *Phys. Rev. Lett.* **105**, 095702 (2010).
  - [3] S. Sachdev, *Quantum Phase Transitions*, 2nd ed. (Cambridge University, Cambridge, England, 2011).
  - [4] M. Huber, M. Perarnau-Llobet, K. V. Hovhannisyán, P. Skrzypczyk, C. Klöckl, N. Brunner, and A. Acín, *New J. Phys.* **17**, 065008 (2015).
  - [5] M. A. Nielsen and I. L. Chuang, *Quantum Computation and Quantum Information* (Cambridge University, Cambridge, England, 2000).
  - [6] I. Bloch, J. Dalibard, and S. Nascimbène, *Nat. Phys.* **8**, 267 (2012).
  - [7] I. M. Georgescu, S. Ashhab, and F. Nori, *Rev. Mod. Phys.* **86**, 153 (2014).
  - [8] M. Afzelius, N. Gisin, and H. de Riedmatten, *Phys. Today* **68**(12), 42 (2015).
  - [9] T. Byrnes, P. Recher, N. Y. Kim, S. Utsunomiya, and Y. Yamamoto, *Phys. Rev. Lett.* **99**, 016405 (2007).
  - [10] V. Giovannetti, S. Lloyd, and L. Maccone, *Science* **306**, 1330 (2004).

- [11] C. You, S. Adhikari, Y. Chi, M. L. LaBorde, C. T. Matyas, C. Zhang, Z. Su, T. Byrnes, C. Lu, J. P. Dowling *et al.*, *J. Opt.* **19**, 124002 (2017).
- [12] I. Urizar-Lanz, P. Hyllus, I. L. Egusquiza, M. W. Mitchell, and G. Tóth, *Phys. Rev. A* **88**, 013626 (2013).
- [13] Y. Jing, M. Fadel, V. Ivannikov, and T. Byrnes, *New J. Phys.* **21**, 093038 (2019).
- [14] R. Jozsa, D. S. Abrams, J. P. Dowling, and C. P. Williams, *Phys. Rev. Lett.* **85**, 2010 (2000).
- [15] E. O. Ilo-Okeke, L. Tessler, J. P. Dowling, and T. Byrnes, *npj Quantum Inf.* **4**, 40 (2018).
- [16] S. Perseguers, J. I. Cirac, A. Acín, M. Lewenstein, and J. Wehr, *Phys. Rev. A* **77**, 022308 (2008).
- [17] S. Broadfoot, U. Dorner, and D. Jaksch, *Phys. Rev. A* **81**, 042316 (2010).
- [18] D. Bohm and Y. Aharonov, *Phys. Rev.* **108**, 1070 (1957).
- [19] D. A. Lidar and T. A. Brun, *Quantum Error Correction* (Cambridge University, Cambridge, England, 2013).
- [20] S. J. Devitt, W. J. Munro, and K. Nemoto, *Rep. Prog. Phys.* **76**, 076001 (2013).
- [21] A. Cabello, *J. Mod. Opt.* **50**, 1049 (2003).
- [22] G. Tóth and M. W. Mitchell, *New J. Phys.* **12**, 053007 (2010).
- [23] M. Horodecki, P. Horodecki, and R. Horodecki, *Phys. Rev. A* **60**, 1888 (1999).
- [24] C. H. Bennett, G. Brassard, S. Popescu, B. Schumacher, J. A. Smolin, and W. K. Wootters, *Phys. Rev. Lett.* **76**, 722 (1996).
- [25] A. N. Pyrkov and T. Byrnes, *Phys. Rev. A* **90**, 062336 (2014).
- [26] T. Byrnes, K. Wen, and Y. Yamamoto, *Phys. Rev. A* **85**, 040306(R) (2012).
- [27] A. Abdelrahman, T. Mukai, H. Häffner, and T. Byrnes, *Opt. Express* **22**, 3501 (2014).
- [28] C. H. Bennett, H. J. Bernstein, S. Popescu, and B. Schumacher, *Phys. Rev. A* **53**, 2046 (1996).
- [29] N. Behbood, G. Colangelo, F. Martin Ciurana, M. Napolitano, R. J. Sewell, and M. W. Mitchell, *Phys. Rev. Lett.* **111**, 103601 (2013).
- [30] N. Behbood, F. Martin Ciurana, G. Colangelo, M. Napolitano, G. Tóth, R. J. Sewell, and M. W. Mitchell, *Phys. Rev. Lett.* **113**, 093601 (2014).
- [31] J. Kong, R. Jiménez-Martínez, C. Troullinou, V. G. Lucivero, G. Tóth, and M. W. Mitchell, *Nat. Commun.* **11**, 2415 (2020).
- [32] A. Cabello, *Phys. Rev. Lett.* **89**, 100402 (2002).
- [33] G.-S. Jin, S.-S. Li, S.-L. Feng, and H.-Z. Zheng, *Phys. Rev. A* **71**, 034307 (2005).
- [34] W.-C. Qiang, W. Cardoso, A. Avelar, and B. Baseia, *Phys. Lett. A* **375**, 443 (2011).
- [35] Z. Chen, Y.-H. Chen, Y. Xia, J. Song, and B.-H. Huang, *Sci. Rep.* **6**, 22202 (2016).
- [36] M. Schimpf and K. Svozil, *Mathematica Slovaca* **60**, 701 (2010).
- [37] S. Chaudhury, S. Merkel, T. Herr, A. Silberfarb, I. H. Deutsch, and P. S. Jessen, *Phys. Rev. Lett.* **99**, 163002 (2007).
- [38] L. M. Norris, C. M. Trail, P. S. Jessen, and I. H. Deutsch, *Phys. Rev. Lett.* **109**, 173603 (2012).
- [39] B. E. Anderson, H. Sosa-Martinez, C. A. Riofrío, I. H. Deutsch, and P. S. Jessen, *Phys. Rev. Lett.* **114**, 240401 (2015).
- [40] P. Böhi, M. F. Riedel, J. Hoffrogge, J. Reichel, T. W. Hänsch, and P. Treutlein, *Nat. Phys.* **5**, 592 (2009).
- [41] M. F. Riedel, P. Böhi, Y. Li, T. W. Hänsch, A. Sinatra, and P. Treutlein, *Nature (London)* **464**, 1170 (2010).
- [42] K. Hammerer, A. S. Sørensen, and E. S. Polzik, *Rev. Mod. Phys.* **82**, 1041 (2010).
- [43] L. Pezzè, A. Smerzi, M. K. Oberthaler, R. Schmied, and P. Treutlein, *Rev. Mod. Phys.* **90**, 035005 (2018).
- [44] Y. Takahashi, K. Honda, N. Tanaka, K. Toyoda, K. Ishikawa, and T. Yabuzaki, *Phys. Rev. A* **60**, 4974 (1999).
- [45] J. M. Higbie, L. E. Sadler, S. Inouye, A. P. Chikkatur, S. R. Leslie, K. L. Moore, V. Savalli, and D. M. Stamper-Kurn, *Phys. Rev. Lett.* **95**, 050401 (2005).
- [46] A. Kuzmich and T. A. B. Kennedy, *Phys. Rev. Lett.* **92**, 030407 (2004).
- [47] R. Meppelink, R. A. Rozendaal, S. B. Koller, J. M. Vogels, and P. van der Straten, *Phys. Rev. A* **81**, 053632 (2010).
- [48] E. O. Ilo-Okeke and T. Byrnes, *Phys. Rev. Lett.* **112**, 233602 (2014).
- [49] E. O. Ilo-Okeke and T. Byrnes, *Phys. Rev. A* **94**, 013617 (2016).
- [50] J. Appel, P. J. Windpassinger, D. Oblak, U. B. Hoff, N. Kjærgaard, and E. S. Polzik, *Proc. Natl. Acad. Sci. USA* **106**, 10960 (2009).
- [51] M. H. Schleier-Smith, I. D. Leroux, and V. Vuletić, *Phys. Rev. Lett.* **104**, 073604 (2010).
- [52] R. J. Sewell, M. Koschorreck, M. Napolitano, B. Dubost, N. Behbood, and M. W. Mitchell, *Phys. Rev. Lett.* **109**, 253605 (2012).
- [53] K. C. Cox, G. P. Greve, J. M. Weiner, and J. K. Thompson, *Phys. Rev. Lett.* **116**, 093602 (2016).
- [54] O. Hosten, N. J. Engelsen, R. Krishnakumar, and M. A. Kasevich, *Nature (London)* **529**, 505 (2016).
- [55] G. Vasilakis, H. Shen, K. Jensen, M. Balabas, D. Salart, B. Chen, and E. S. Polzik, *Nat. Phys.* **11**, 389 (2015).
- [56] C. B. Møller, R. A. Thomas, G. Vasilakis, E. Zeuthen, Y. Tsaturyan, M. Balabas, K. Jensen, A. Schliesser, K. Hammerer, and E. S. Polzik, *Nature (London)* **547**, 191 (2017).
- [57] J. E. Aristizabal-Zuluaga, I. Skobleva, L. Richter, Y. Ji, Y. Mao, M. Kondappan, V. Ivannikov, and T. Byrnes, *J. Phys. B* **54**, 105502 (2021).
- [58] E. O. Ilo-Okeke, S. Sunami, C. J. Foot, and T. Byrnes, *Phys. Rev. A* **104**, 053324 (2021).
- [59] A. Kuzmich, L. Mandel, and N. P. Bigelow, *Phys. Rev. Lett.* **85**, 1594 (2000).
- [60] E. O. Ilo-Okeke and T. Byrnes, Measurement operator formalism for quantum nondemolition measurements (unpublished).
- [61] G. T. Genov, D. Schraft, T. Halfmann, and N. V. Vitanov, *Phys. Rev. Lett.* **113**, 043001 (2014).
- [62] Y. Mao, M. Chaudhary, M. Kondappan, J. Shi, E. O. Ilo-Okeke, V. Ivannikov, and T. Byrnes, [arXiv:2202.09100](https://arxiv.org/abs/2202.09100).
- [63] C. Radhakrishnan, Z. Ding, F. Shi, J. Du, and T. Byrnes, *Annal. Phys. (NY)* **409**, 167906 (2019).
- [64] Z.-H. Ma, J. Cui, Z. Cao, S.-M. Fei, V. Vedral, T. Byrnes, and C. Radhakrishnan, *Europhys. Lett.* **125**, 50005 (2019).
- [65] F. T. Arecchi, E. Courtens, R. Gilmore, and H. Thomas, *Phys. Rev. A* **6**, 2211 (1972).
- [66] M. Karski, L. Förster, J. M. Choi, W. Alt, A. Widera, and D. Meschede, *Phys. Rev. Lett.* **102**, 053001 (2009).
- [67] W. Zhou, M. P. Oxley, A. R. Lupini, O. L. Krivanek, S. J. Pennycook, and J. Idrobo, *Microsc. Microanal.* **18**, 1342 (2012).
- [68] A. Alberti, C. Robens, W. Alt, S. Brakhane, M. Karski, R. Reimann, A. Widera, and D. Meschede, *New J. Phys.* **18**, 053010 (2016).

- [69] S. Gao, E. O. Ilo-Okeke, Y. Mao, M. Kondappan, J. E. Aristizabal-Zuluaga, V. Ivannikov, and T. Byrnes, *J. Phys. B At. Mol. Opt. Phys.* **55**, 195501 (2022).
- [70] B. Julsgaard, A. Kozhekin, and E. S. Polzik, *Nature (London)* **413**, 400 (2001).
- [71] R. Grimm and M. Weidemüller, *Adv. At. Mol. Opt. Phys.* **42**, 95 (1978).
- [72] M. Q. Lone and T. Byrnes, *Phys. Rev. A* **92**, 011401(R) (2015).
- [73] H. Zhang, R. McConnell, S. Čuk, Q. Lin, M. H. Schleier-Smith, I. D. Leroux, and V. Vuletić, *Phys. Rev. Lett.* **109**, 133603 (2012).
- [74] S. Colombo, E. Pedrozo-Peñañiel, A. F. Adiyatullin, E. Mendez, C. Shu, and V. Vuletić, *Nat. Phys.* **18**, 925 (2022).
- [75] A. Cabello, *Phys. Rev. A* **68**, 012304 (2003).